Available online at www.sciencedirect.com

SCIENCE DIRECT®

Journal of Molecular Catalysis A: Chemical 204–205 (2003) 509–518

JOURNAL OF MOLECULAR CATALYSIS A: CHEMICAL

www.elsevier.com/locate/molcata

Characterization and catalytic performances of alkali-metal promoted Rh/SiO_2 catalysts for propene hydroformylation

Laura Sordelli [a,*], Matteo Guidotti [a], Daniele Andreatta [b], Gilberto Vlaic [b,c], Rinaldo Psaro [a]

[a] *CNR–ISTM, Istituto di Scienze e Tecnologie Molecolari, via C. Golgi 19, 20133 Milano, Italy*
[b] *Dip. Scienze Chimiche, Universita' di Trieste, Via L.Giorgieri 1, 34127 Trieste, Italy*
[c] *Sincrotrone Trieste SCpA and Laboratorio Nazionale TASC-INFM, Area Science Park, SS 14 Km.163.5, 34012 Basovizza, Italy*

Received 5 November 2002; received in revised form 8 February 2003; accepted 22 February 2003

Dedicated to Professor Renato Ugo on the occasion of his 65th birthday

Abstract

The influence of the cationic promoters (M = Li, Na, K, Rb, Cs) on silica-supported rhodium catalysts was examined in the hydroformylation of propene at 413 K and atmospheric pressure. The catalysts were prepared by aqueous co-impregnation of $RhCl_3 \cdot 3H_2O$ and alkali-metal chloride. The rhodium to promoter molar ratio was 1. A pre-treatment cycle under $O_2/H_2/O_2$ at 673 K was carried out on the catalyst before the admission of the hydroformylation mixture. By in situ Rh K-edge extended X-ray adsorption fine-structure (EXAFS) characterization of the activated catalyst, two different Rh and alkali-metal oxide phases, highly dispersed and in intimate contact with each other, were detected on the support surface. Under catalytic conditions, small Rh metal particles are formed, with a mean diameter of 3.2 nm, as detected by HRTEM. The activity in aldehyde formation depends on the alkali-metal promoter in the following order: Li > Na > K > Rb ≫ Cs. This behavior parallels the trend of the polarizing power of the cation within the Group 1.

Keywords: Promotion effect; Propene hydroformylation; Rh catalysts; Silica; EXAFS characterization

1. Introduction

In last decades, many efforts have been made in the preparation of a heterogeneous catalyst for the hydroformylation of light alkenes with performances at least comparable to those obtained with homogeneous systems [1,2]. Leaving out the immobilization or heterogenization of active transition-metal complexes on solid carriers, many examples of deposition of metal precursors on amorphous, microporous or mesoporous inorganic oxides have been reported [3]. In such studies, rhodium is by far the most widely used metal. Nevertheless, in the vapor-phase reaction most of the monometallic catalysts display a low total activity together with a low chemoselectivity to oxygenated products. A remarkable improvement of the catalytic performances has been obtained by doping the catalyst surface with sulphur [4,5] or selenium [6], by adding promoters, as alkali metals [7–9], zinc [10] or boron [11,12], and by using bimetallic systems, e.g. Rh-Co [13,14], Rh-Mo [15], Rh-Fe [16,17]. In a previous study, the influence of the cationic promoters on rhodium was examined in the hydroformylation

* Corresponding author. Fax: +39-02-503-14405.
E-mail address: lauras@csmtbo.mi.cnr.it (L. Sordelli).

1381-1169/$ – see front matter © 2003 Elsevier Science B.V. All rights reserved.
doi:10.1016/S1381-1169(03)00333-9

of ethene using silica-supported $M_2[Rh_{12}(CO)_{30}]$ (M = Li, Na, K) species, in which the promoting cation was present in the coordination sphere of the precursor cluster [8]. In this contribution, the catalytic systems were prepared by direct impregnation of the traditionally used chloride salts of both rhodium and the promoter, respectively. Moreover, in order to have an insight also into the regioselective properties, the catalysts were tested in the hydroformylation of propene. We present also a detailed investigation of the structural properties of the rhodium surface chemistry resulting from the pre-treatments, as determined by in situ EXAFS spectroscopy.

2. Experimental

2.1. Catalysts preparation

SiO_2 (Grace Davison 62; mean pore diameter and specific surface area 14 nm and 357 $m^2\,g^{-1}$, respectively), ground and washed with 1 M HNO_3 and with demonized water to neutrality, was used as a support. The rhodium-containing catalysts were prepared by impregnation or co-impregnation of the support using an aqueous solution of $RhCl_3{\cdot}3H_2O$ (Engelhard) and, eventually, an aqueous solution of a metal chloride MCl (M = Li, Na, K, Rb, Cs; Carlo Erba). After drying, the samples were stored under N_2. All the samples had a rhodium loading of 2.0 ± 0.1 wt.% (AA spectroscopy measurement). The rhodium to promoter molar ratio was 1 in all the samples (M/Rh = 1).

The chlorine content was determined by potentiometric titration of Cl^- with $AgNO_3$ [18] after each activation step and after a 20 h-catalysis run for all samples (2% Rh loading). In order to get higher spectral signal-to-noise ratio, some samples used in the EXAFS characterization had a rhodium loading of 4.0 ± 0.1 wt.% (after checking the overlapping with the corresponding 2% loading samples).

2.2. Catalytic studies

A series of previous catalytic tests, performed by varying the promoter content with respect to rhodium, allowed to establish that the M/Rh value of 1 displays the best catalytic performances. All the samples underwent a calcination (O_2; 10 ml min^{-1}; 1 h), reduction (H_2; 10 ml min^{-1}; 1 h) and calcination (O_2; 10 ml min^{-1}; 1 h) pre-treatment at 673 K before reaction mixture admission.

The hydroformylation of propene was carried out in a fixed-bed continuous-flow glass reactor (typical load = 320 mg of catalyst) at 413 K, at atmospheric pressure and at a total gas flow of 15 ml min^{-1} (C_3H_6:CO:H_2 = 0.5:1:1 molar ratio; contact time = 39 s). Quantitative analysis was performed with GC-FID instrumentation (HP 5890A) equipped with a Poraplot Q column (0.53 mm i.d.; 25 m length). Reported activity and selectivity were evaluated after 20 h on stream, when all the systems reached the steady state. In order to operate in differential mode, the catalytic parameters were tuned so to keep the total propene conversion $\leq$1%.

2.3. HRTEM characterization

The high resolution electron microscopy (HRTEM) study has been performed on a JEOL 2000 electron microscope, operating at 200 kV. The samples were micro-dispersed in *iso*-propanol by ultrasounds. A drop of the suspensions was deposited on a carbon-covered copper grid and the solvent was evaporated. Before the analysis, the samples were kept in UHV overnight. Micrographs were taken at 340,000× magnification.

2.4. EXAFS characterization

EXAFS transmission measurements were carried out at the XAS-13 station of the DCI ring at LURE (Orsay, France), using a Si(331) channel-cut monochromator. Rh metal foil has been used for the angle/energy calibration.

All spectra were recorded at 300 K in transmission mode at the Rh K-edge over the range 23–24.2 keV, with a sampling step of 2 eV and an integration time of 2 s for each point. Incident and transmitted photon fluxes have been detected with ionization chambers filled, respectively, with 0.1 and 0.4 bar of Kr. Each spectrum had been acquired three times in order to perform the statistical analysis and average the extracted EXAFS oscillation, so increasing the signal-to-noise ratio. The powder samples were loaded under inert atmosphere, and treated in situ inside a catalysis-EXAFS

cell (Lytle type), and cooled down to room temperature before spectra acquisition.

Extracted $\chi(k)$ data had been averaged before the EXAFS data analysis. Standard deviation calculated from the averaged spectra was used as an estimate of the statistical noise for the evaluation of the errors associated with each structural parameter [19]. Experimental $\chi(k)$ data were extracted from absorption data by a conventional procedure [20]. The k^3-weighted $\chi(k)$ data were Fourier transformed over a typical k range of 3–14 $Å^{-1}$ and main contributions to the Fourier transform modulus were filtered in order to obtain metal nearest-neighbor shells. The so obtained filtered contributions were analyzed using the programs developed by Michalowicz [21] whose non-linear least-squares fit exploits the minimization capabilities of the MINUIT program [22]. Phase shift and amplitude functions of scattering atoms have been extracted from the experimental spectra of the following model compounds: Rh foil, Rh_2O_3 and $RhCl_3/SiO_2$ (10 wt.% in Rh). It is not possible to detect the Li scatterers, since the scattering amplitude is very low. Whenever necessary the statistical significance of the results obtained was checked by applying the *F*-test proposed by Joyner et al. [23].

3. Results and discussion

In our previous studies, with cluster-derived rhodium catalysts prepared from salts (Li^+, Na^+, K^+) of the cluster anion $[Rh_{12}(CO)_{30}]^{2-}$ supported on silica, remarkable effects on the activity and selectivity to propanal were induced only upon a catalysts pre-treatment in O_2 at 773 K. A simple exposure to the hydroformylation mixture at 393 K was enough to generate the active metallic phase [24].

In the present study, the catalysts were prepared by using the chloride salts of both rhodium and alkali promoter. In order to optimize the chlorine removal in the fresh catalyst and to form a highly dispersed Rh_2O_3 phase, the residual chloride amount on the catalyst was evaluated after each step of the pre-treatment cycle. The titration results are reported in Table 1. The residual chloride amount on the catalysts at the end of the $O_2/H_2/O_2$ pre-treatment cycle at 673 K was negligible. Significant amounts of chlorine were still present only on the Li/Rh = 5 system.

Table 1
Chloride residue on the catalysts after each pre-treatment step at 673 K (reference: fresh catalyst corresponds to 100%)

Catalyst	O_2	O_2/H_2	$O_2/H_2/O_2$
Rh/SiO_2	80	7	–
$Rh\text{-}Li/SiO_2$, Li/Rh = 1	32	6	–
$Rh\text{-}Li/SiO_2$, Li/Rh = 5	72	51	44

3.1. Catalytic properties

The vapor-phase propene hydroformylation on Rh/SiO_2, under the present conditions, is governed by two parallel reactions: hydrogenation to propane and hydroformylation to C_4 aldehydes. No detectable formation of C_4 alcohols was registered. The non-promoted catalyst Rh/SiO_2, activated with a $O_2/H_2/O_2$ treatment at 673 K, showed a good hydrogenating activity to propane together with the production of oxygenated compounds (*n*-butanal and *iso*-butanal), as reported in Table 2. All of the catalytic systems promoted by alkali metals gave rise to efficient systems with better activity and selectivity performances than the non-promoted one (Table 2). In particular, the promoting effect was maximum with lithium and decreased gradually descending in the Group 1 metals, from sodium to cesium. The presence of Li, in the molar ratio 1:1, promoted mainly the hydroformylation reaction: the aldehyde formation rate on the Li-containing sample was six times higher than the non-promoted one, while the chemo-selectivity to oxygenated compounds was only ca. 50% higher. The performances of the $Rh\text{-}Li/SiO_2$ sample are reported in Fig. 1. On the opposite, the addition of Cs resulted in a deactivation of both the hydrogenation and hydroformylation activity. An excess of promoting metal caused a drop of the total conversion and indeed the sample with a Li/Rh ratio = 5 was completely inactive towards both hydrogenation and hydroformylation. With respect to the regioselectivity, on all of the catalysts the formation of *n*-butanal was favored and only a slight improvement was observed passing from lithium to cesium. Some tests were run with long reaction times up to 150 h, to check the stability of the catalysts. In all of these cases, no noteworthy deactivation was recorded and both activity and selectivity reached steady values after the first 15 h on stream (Fig. 1).

Table 2
Hydroformylation of propene

Catalyst	Total conversion (%)[a]	Rate[b] ($\times 10^3$)			Selectivity (%)			
		C_3H_8	*i*-CHO[c]	*n*-CHO[d]	OXY[e]	Regio[f]	*i*-CHO[c]	*n*-CHO[d]
Rh/SiO_2	0.20	2.32	0.51	1.16	42	70	13	29
$Rh\text{-}Li/SiO_2$	0.85	7.26	2.89	7.70	59	73	16	43
$Rh\text{-}Li/SiO_2$[g]	<0.05	–	–	–	–	–	–	–
$Rh\text{-}Na/SiO_2$	0.54	6.00	1.13	4.34	48	79	10	38
$Rh\text{-}K/SiO_2$	0.55	5.92	1.32	4.33	48	77	11	37
$Rh\text{-}Rb/SiO_2$	0.34	4.15	0.72	2.86	46	80	9	37
$Rh\text{-}Cs/SiO_2$	<0.05	–	–	–	–	–	–	–

Values after 20 h on stream. Conditions: 413 K; C_3H_6:CO:H_2 = 0.5:1:1; 15 ml min^{-1} total flow; 1 bar; Rh = 2 wt.%, M/Rh = 1.
[a] Total conversion based on propene consumption (%).
[b] Rate of formation (mol $[min]^{-1}$ $[mol_{Rh}]^{-1}$).
[c] *i*-CHO: *iso*-butanal.
[d] *n*-CHO: *n*-butanal.
[e] Selectivity to oxygenated products (aldehydes).
[f] Regioselectivity as ratio $n/(n + iso)$.
[g] Li/Rh molar ratio = 5.

3.2. Structural characterization

The EXAFS analysis has been performed on the monometallic $RhCl_3/SiO_2$ and on the more active $RhCl_3$-LiCl/SiO_2 catalysts (molar ratio Li/Rh = 1 and 5, for a comparison with a Li excess system as a model of a totally inactive promoted catalyst) after each step of the pre-treatment cycle, after exposure

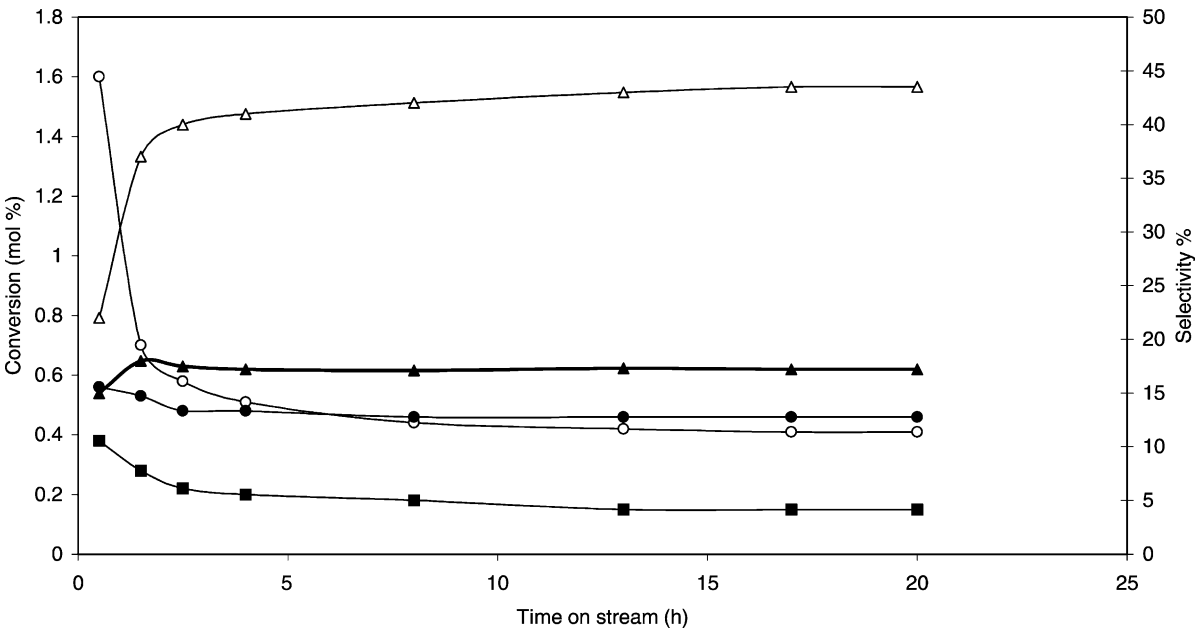

Fig. 1. Catalytic performances of $Rh\text{-}Li/SiO_2$ sample vs. time in the hydroformylation of propene. Conditions: 413 K, C_3H_6:CO:H_2 = 0.5:1:1, 15 ml min^{-1} total flow, 1 bar, Rh = 2 wt.%, M/Rh = 1. Catalysts pre-treatment: $O_2/H_2/O_2$ at 673 K. (●) *n*-Butanal conversion; (○) propane conversion; (■) *i*-butanal conversion; (▲) selectivity to *i*-aldehyde; (△) selectivity to *n*-aldehyde.

Table 3
Curve fitting results of the Rh K-edge EXAFS data

Sample[a]	Treatment[b]	Shell	CN	R (Å)	$\Delta\sigma$ (Å) $\times 10^2$	ΔE_o (eV)	Δk (Å^{-1})[e]	ΔR (Å)[f]
Rh/SiO_2	Fresh	Cl	5.7 ± 0.2	2.300 ± 0.002	7.0 ± 0.3	3.8 ± 0.2	3.0–14.0	1.2–2.5
Rh/SiO_2	O_2	O	4 ± 0.1	2.002 ± 0.002	7.2 ± 0.4	−3.4 ± 1.0	3.0–14.0	1.2–3.1
		Cl	1.3 ± 0.1	2.330 ± 0.002	8.2 ± 0.3	4.7 ± 0.7		
Rh/SiO_2	O_2–H_2	Rh	10.5 ± 0.3	2.692 ± 0.002	7.6 ± 0.1	0.4 ± 0.1	3.0–14.0	1.8–2.9
Rh/SiO_2	O_2–H_2–O_2	O	5.3 ± 0.3	2.012 ± 0.003	8.8 ± 0.5	1.6 ± 0.1	3.0–14.0	1.2–2.1
Rh/SiO_2	CO/H_2[c]	Rh	10.7 ± 0.3	2.692 ± 0.002	7.7 ± 0.1	0.3 ± 0.2	3.0–14.0	1.8–2.9
Rh-Li/SiO_2	Fresh	Cl	5.9 ± 0.1	2.303 ± 0.002	6.6 ± 0.2	1.4 ± 0.2	3.0–14.0	1.3–2.5
Rh-Li/SiO_2	O_2	O	2.1 ± 0.5	2.055 ± 0.015	7.0 ± 1.0	2.7 ± 0.8	3.0–14.0	1.3–2.5
		Cl	3.9 ± 0.9	2.30 ± 0.03	7.0 ± 1.0	1.8 ± 0.5		
Rh-Li/SiO_2	O_2–H_2	Rh	6.8 ± 0.3	2.722 ± 0.002	10.6 ± 0.2	−4.7 ± 0.2	3.0–14.0	1.3–2.9
Rh-Li/SiO_2	O_2–H_2–O_2	O	6.0 ± 0.1	2.012 ± 0.001	10.4 ± 0.1	4.5 ± 0.1	3.0–12.0	0.9–2.2
Rh-Li/SiO_2	CO/H_2[c]	O	1.0 ± 0.5	2.076 ± 0.005	9.4 ± 0.4	3.7 ± 0.1	3.0–14.0	1.4–2.9
		Rh	7.7 ± 0.3	2.746 ± 0.003	11.4 ± 0.4	3.5 ± 0.5		
Rh-Li/SiO_2	Used	O	1.5 ± 0.5	2.060 ± 0.005	9.4 ± 0.4	3.7 ± 0.1	3.0–12.0	0.9–2.2
		Rh	5.7 ± 0.3	2.699 ± 0.003	8.5 ± 0.4	−3.5 ± 0.5		
Rh-Li/SiO_2[d]	Fresh	O	1.2 ± 0.5	2.05 ± 0.01	7.0 ± 1.0	2.7 ± 0.8	3.0–14.0	1.3–2.5
		Cl	5.0 ± 0.9	2.31 ± 0.03	7.0 ± 1.0	1.8 ± 0.5		
Rh-Li/SiO_2[d]	O_2	O	1.9 ± 0.1	2.005 ± 0.005	7.2 ± 0.4	−3.4 ± 1.0	3.0–14.0	1.4–2.4
		Cl	2.3 ± 0.1	2.330 ± 0.004	8.2 ± 0.3	4.7 ± 0.7		
Rh-Li/SiO_2[d]	O_2–H_2	O	1.0 ± 0.5	2.076 ± 0.005	9.4 ± 0.4	3.7 ± 0.1	3.0–14.0	1.3–2.9
		Rh	7.7 ± 0.3	2.746 ± 0.003	11.4 ± 0.4	3.5 ± 0.5		
Rh-Li/SiO_2[d]	O_2–H_2–O_2	O	6.0 ± 0.1	2.012 ± 0.001	10.4 ± 0.1	4.5 ± 0.1	3.0–12.0	1.0–2.2

[a] Rh loading: 4 wt.%; Li/Rh molar ratio: 1 (unless otherwise reported).
[b] At 673 K (unless otherwise reported).
[c] At 413 K.
[d] Li/Rh molar ratio = 5.
[e] FFT and k-fit range.
[f] FFT^{-1} range (not phase corrected).

to CO/H_2 at 413 K, and after a 20 h-catalysis run. Best-fit results are reported in Table 3.

3.2.1. Rh/SiO_2

The comparison of the FT spectrum of the just impregnated $RhCl_3/SiO_2$ (4 wt.%) sample (Fig. 2) with the reference used for rhodium chloride ($RhCl_3/SiO_2$, 10 wt.%), shows their complete overlay. The only large peak at about 2.3 Å corresponds to the Cl shell. The fit calculated over the filtered range ΔR = 1–3 Å gives 5.7 Cl atoms at 2.300 Å. By simple impregnation all the rhodium is still present as $RhCl_3$. After the first calcination treatment at 672 K, a three shell structure (Rh-O, Rh-Cl and Rh-Rh) occurs. The comparison with the crystal data of rhodium salt and rhodium oxide shows that the sample structure corresponds to a mixed phase where part of the rhodium is still present as chloride and part as oxide or, possibly, oxochloride species. After the reduction at 673 K, the FT spectrum exhibits all the features of the rhodium foil up to the fourth shell (Fig. 2) and the first shell fit gives 10.5 Rh atoms at 2.692 Å. That means small rhodium metal particles with fcc structure. No chlorine is detected any more. A further in situ calcination at 673 K produces a completely oxidized rhodium, where the first shell fit gives values coincident with those of Rh_2O_3. After the reduction at 413 K in the CO/H_2 mixture, the FT spectrum exhibits the same features than after the high temperature hydrogen reduction and the first shell fit gives 10.7 Rh atoms at 2.692 Å, that means that small Rh metal particles are formed with the same structure and dispersion degree as after reduction.

3.2.2. Rh-Li/SiO_2

The comparison between the FT spectra of the freshly impregnated Rh-Li/SiO_2 sample (Fig. 2) and

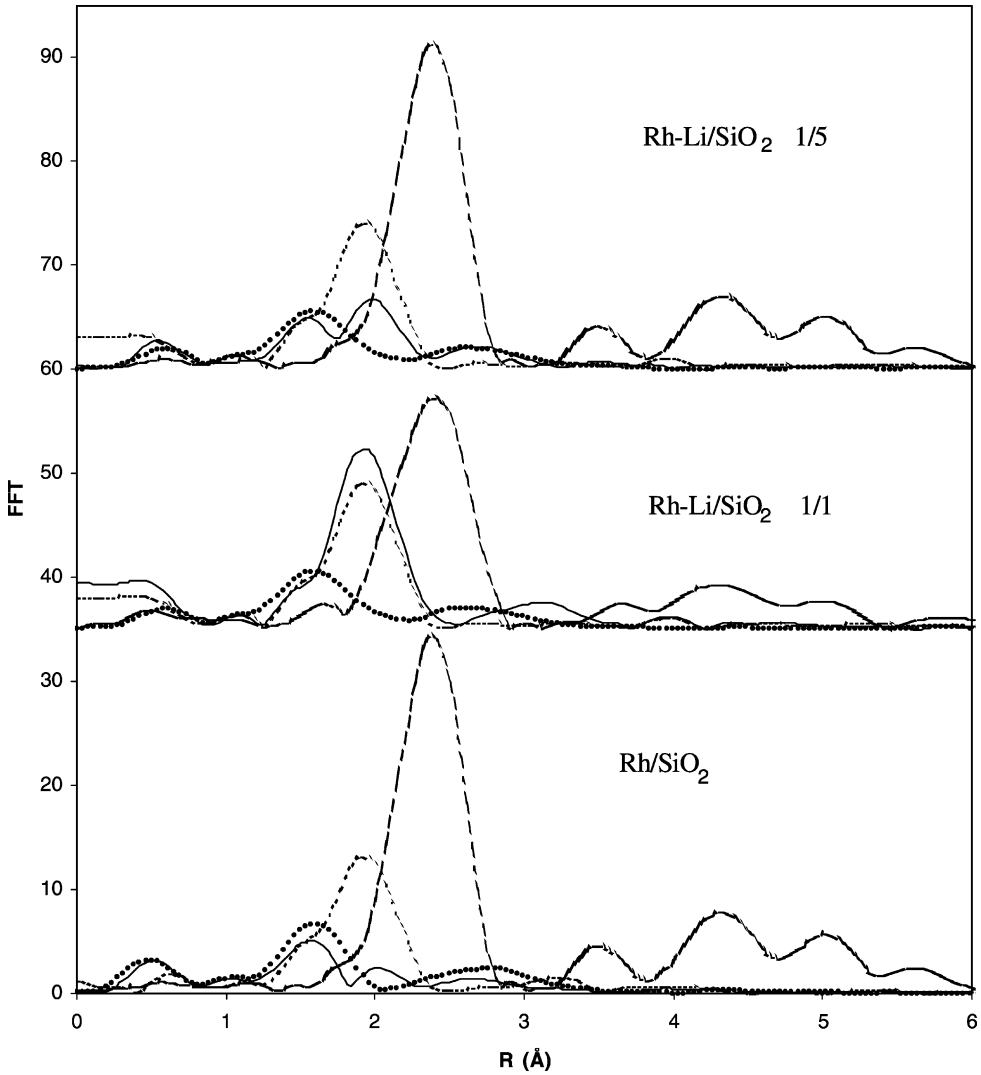

Fig. 2. Fourier transform moduli of the Rh K-edge k^3-weighted EXAFS data of Rh/SiO_2, Rh-Li/SiO_2 Li/Rh = 1 and of Rh-Li/SiO_2 Li/Rh = 5 after the following steps: (a) impregnation (···); (b) calcination (—); (c) calcination-reduction (- - -) and (d) calcination-reduction-calcination (●●●●).

the $RhCl_3/SiO_2$ reference, shows that the presence of LiCl does not significantly affect the chemical surrounding of rhodium atoms. The best fit for the inverse Fourier Transform of the first peak filtered region, $\Delta R = 1.21–2.39$ Å, reveals the presence of a single shell of six chlorine atoms around the rhodium absorber at almost the same distance as in the $RhCl_3$ crystal (2.303 Å versus 2.310 Å). The FT spectrum of the same sample after oxidation, shown in Fig. 2, exhibits a strong large peak, at about the same distance than Rh-Cl in $RhCl_3$ crystal, which is due to a not well resolved overlap of 2 O atom shell at 2.055 Å and a 4 Cl atoms shell at 2.31 Å. As in the case of the Rh/SiO_2 sample, the structure after calcination corresponds to a mixed phase where part of the Rh is still present as chloride and part as oxide, now with a dominant chloride contribution respect to the oxide. No contribution

from Li oxide is detectable in the nearest Rh surrounding.

The Rh-Li/SiO_2 Li/Rh = 5 sample after impregnation shows a large first peak due to the overlap of an O and a Cl shell, both species at distances comparable to the corresponding oxide and chloride compounds, which suggest the contemporary presence of the two species since from the impregnation step. The Rh-Li/SiO_2 Li/Rh = 5 sample after calcination shows two distinct peaks (Fig. 2) which correspond to Rh-O in the Rh oxide and Rh-Cl in the Rh chloride. The fit obtained on the basis of a two shell model reaches the best quality factor for 1.9 O at 2.005 Å (to be compared with the 2.048 Å in the Rh_2O_3) and 2.3 Cl at 2.330 Å (versus the 2.310 Å of the $RhCl_3$), for a total of six neighbors around the rhodium atom. The low intensity of the FT spectrum is due to the phase opposition between O and Cl as scatterers, which produces destructive interference.

After the reduction at 673 K, the FT spectrum of Rh-Li/SiO_2 exhibits all the features of the Rh foil up to the fourth shell (Fig. 2), and the first shell fit gives 6.8 Rh atoms at 2.722 Å, that means small Rh metal particles with fcc structure. The introduction of an O shell, to include the possible presence of the support, gives a fit statistically not more significant, as evaluated by the *F*-test. The longer Rh-Rh distance than in the foil (2.722 Å versus 2.692 Å) can be assigned to some interstitial Li inside the frame of Rh metal particles. The Rh-Li/SiO_2 Li/Rh = 5 sample after reduction (Table 3) has a Rh neighbors shell (N = 7.7) corresponding to slightly bigger metal particles with still some O or Cl contribution at 2.076 Å (the introduction of an additional shell, to include both the presence of the support and of the Cl residue, gives a fit statistically not more significant than the two shells one). The further elongation of the Rh-Rh distance than in the Li/Rh = 1 sample (2.746 Å versus 2.722 Å) is consistent with the higher Li loading of this sample, a larger fraction of which can be now interstitial inside the frame of Rh metal particles.

The second in situ calcination at 673 K on both Rh-Li/SiO_2 catalysts, produces completely oxidized rhodium species, where the first shell best fit gives values coincident with those of Rh_2O_3. In Fig. 3 is shown the comparison of the FT moduli between the Rh-Li/SiO_2 and Rh/SiO_2 catalysts after in situ reduction in CO/H_2 at 413 K, following the pre-treatment. The two spectra have some resemblance in the Rh peak, but on the Li-promoted sample there is an evident interaction with the support (presence of an O contribution) and no more correspondence between the outer metal shells. The fit of the first shell gives and 7.7 Rh atoms at 2.746 Å plus 1 O atom at 2.076 Å for Rh-Li/SiO_2 versus 10.7 Rh neighbors at 2.692 Å for Rh/SiO_2. Noticeably the comparison between the Rh-Li/SiO_2 samples after the CO/H_2 reduction treatment and after the catalysis run (Fig. 3) shows that smaller metal particles in contact with the support are formed under catalytic ($CO/H_2/C_3H_6$) conditions, with 5.7 Rh neighbors at 2.699 Å and 1.5 O at 2.06 Å. From the Rh-Rh distance it seems that after catalysis there is no more interstitial lithium inside the metal crystal frame.

The metal particles have also been characterized by HRTEM microscopy. The Rh-Li/SiO_2 (Rh 2 wt.%, Li/Rh = 1) catalyst pre-treated in $O_2/H_2/O_2$ at 673 K and was observed after either a reduction treatment in CO/H_2 mixture at 413 K or a catalysis run (in CO/H_2/propene) at 413 K. The histograms of the metal particle size distribution are compared in Fig. 4. After the CO/H_2 reduction the Rh-Li/SiO_2 sample showed an average particle diameter = 4.8 nm; on the other hand, the sample treated in CO/H_2/propene at 413 K displayed a mean diameter = 3.2 nm.

3.3. Relationship between structure and catalytic properties

On the basis of EXAFS data, the global effect of the $O_2/H_2/O_2$ pre-treatment cycle appears to be: (i) the formation of highly dispersed Rh_2O_3 without any surface contamination by chlorine; (ii) the reductive carbonylation of Rh_2O_3 upon admission of the hydroformylation or CO/H_2 mixture at 413 K, leading to the formation of metallic particles. However, the comparison of the results of the exposure to CO/H_2 mixture of the non-promoted Rh/SiO_2 with the promoted system, shows that different surface restructurings take place: Rh metal particles, with no visible contribution from the oxygen, were present in the non-promoted sample, meanwhile smaller particles, strongly interacting with the support and with some small lithium oxide ensembles, were detected for the promoted system. In fact, after the $O_2/H_2/O_2$ treatment two different Rh and Li

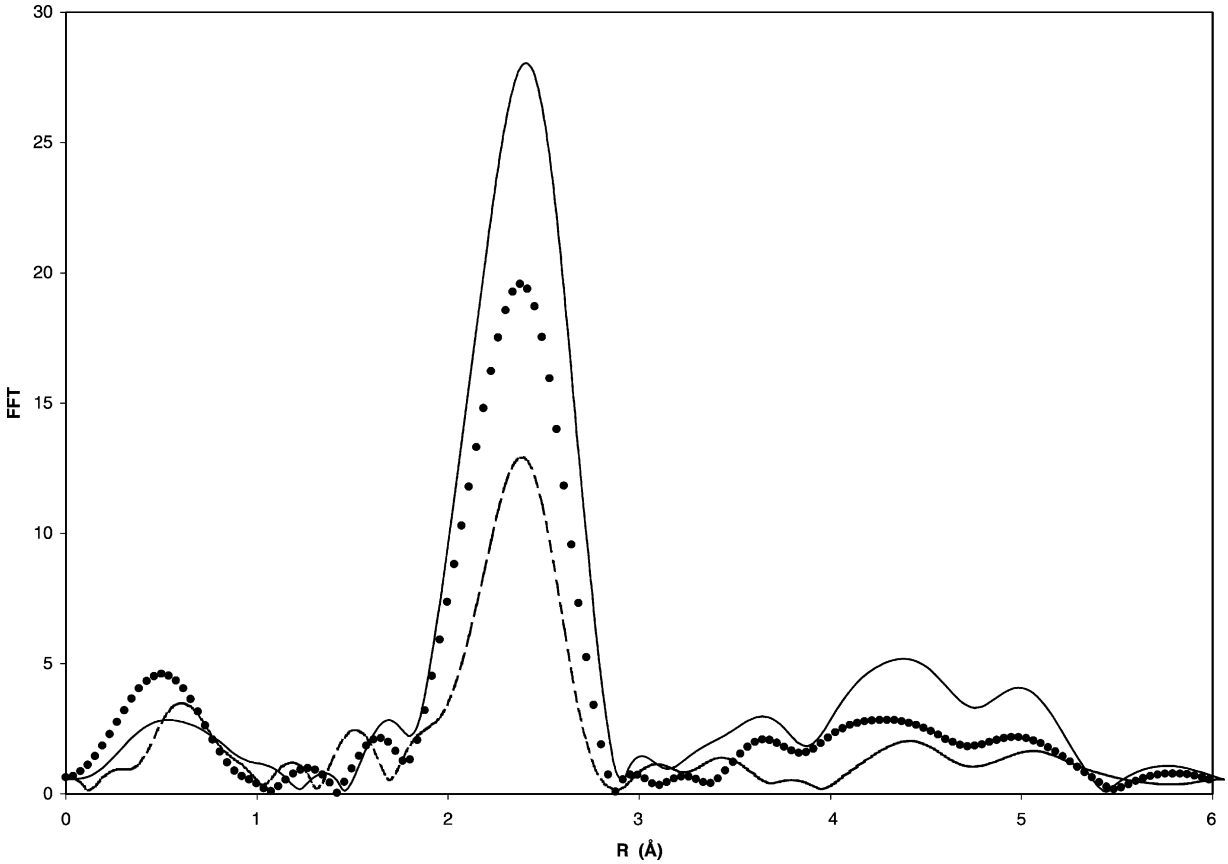

Fig. 3. Fourier transform moduli of the Rh K-edge k^3-weighted EXAFS data of $O_2/H_2/O_2$ pre-treated: Rh-Li/SiO_2 (●●●●) and Rh/SiO_2 (—) after in situ reduction in CO/H_2 at 413 K, and of Rh-Li/SiO_2 (- - -) after catalysis.

oxide phases are likely to be formed, highly dispersed and in intimate contact with each other. In this way small metal domains are closely in contact, or covered by, small oxidic aggregates. At Li/Rh = 1 ratio the two phases have a large common surface and so the reaction may occur at this interphase. Whenever the promoter/metal ratio is higher (as in Li/Rh = 5), the covering effect prevails with a consequent decrease of the active sites number, as reported elsewhere [25]. It is thus evident that, after the almost complete chlorine removal via O_2/H_2 treatment, the subsequent calcination is a crucial step to have an effective contact between the rhodium and lithium phases. Then, the following in situ reduction with the reaction mixture (H_2 + CO + propene) leads to the surface restructuring of the rhodium oxide into the catalytically active species. Consistently to such a hypothesis, on the Rh-Li/SiO_2 sample, which underwent a simple O_2/H_2 pre-treatment, rhodium metal particles were observed, but they exhibited a very low catalytic activity (total conversion <0.05%).

In the most accredited picture of the promotion mechanism, the alkali-metal promoter is present as "patches" of oxide at the surface of the metal particles and the process occurs at the metal/oxide interface [26,27]. Actually, with these systems, it is worth noting that the presence of lithium enhances the selectivity to oxygenated compounds, but it does not suppress the hydrogenation activity. Rather, it promotes both hydrogenation and hydroformylation in a different ratio. Therefore, according to the model proposed by Sachtler et al. [10,16], there is an interaction between the carbonyl group and the cation of the alkali oxide, which is similar to those observed in the Lewis

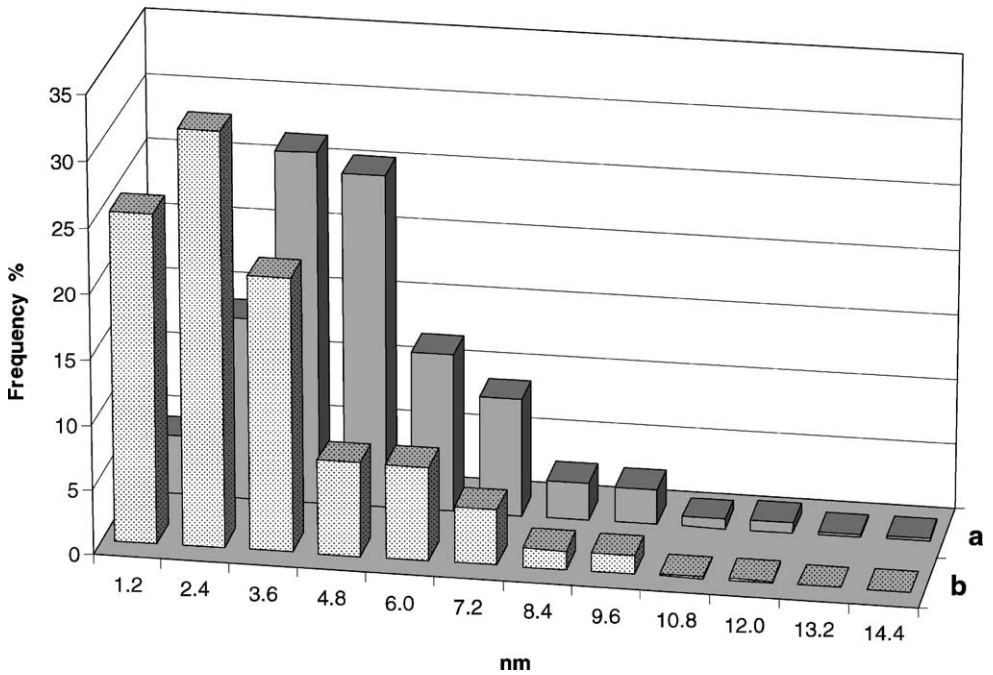

Fig. 4. Histograms of metal particle size distribution, as measured by HRTEM micrographs of Rh-Li/SiO_2 (Rh 2 wt.%, Li/Rh = 1) catalyst, pre-treated in $O_2/H_2/O_2$ at 673 K, after: (a) CO/H_2 reduction at 413 K, (b) $CO/H_2/C_3H_6$ treatment at 413 K.

acid–base couples in solution [28]. Such an interaction appears to increase the rate of CO insertion, as indicated by the enhancement in selectivity for butanal formation. Moreover, in our results, the total activity decreased constantly passing from lithium to cesium in the following order:

$$Li > Na > K > Rb \gg Cs$$

This behavior parallels the trend of the polarizing power of the cation within the Group 1. The lower the polarizing effect of the metal, the smaller is the promoting effect in hydroformylation. In fact, it is also consistent with the Lewis acid–base model: the more polarizing the cation, the more acidic the promoter and the greater is the enhancement of the aldehyde formation.

4. Conclusions

The use of aqueous co-impregnation of chloride salts of both rhodium and alkali metal promoter, as precursor of active supported metal catalysts, is strictly connected to the pre-treatments applied to the freshly prepared catalysts. After the $O_2/H_2/O_2$ treatment two different Rh and alkali metal oxide phases, highly dispersed and in intimate contact with each other, were obtained. This oxidic interphase is likely to be the factor responsible for the promotion effect of the catalytically active species generated by reductive carbonylation under catalytic conditions. Among alkali metals, lithium is the most favorable to aldehyde formation.

Acknowledgements

We acknowledge the support and the use of the facility of the LURE synchrotron laboratory in Orsay (Paris) and thank the staff of the XAS-13 beamline for their assistance. We thank Prof. Coluccia for the access to the HRTEM instrument of IFM Chemistry Department of Torino University, and Prof. Martra for his assistance.

References

[1] M. Beller, B. Cornils, C.D. Frohning, C.W. Kohlpaintner, J. Mol. Catal. A 104 (1995) 17.
[2] F. Joò, E. Papp, A. Kathò, Top. Catal. 5 (1998) 113.
[3] M. Lenarda, L. Storaro, R. Ganzerla, J. Mol. Catal. A 111 (1996) 203 (see also references therein).
[4] Y. Konishi, M. Ichikawa, W.M.H. Sachtler, J. Phys. Chem. 91 (1987) 6286.
[5] S.S.C. Chuang, S.I. Pien, J. Mol. Catal. 55 (1989) 12.
[6] Y. Izumi, K. Asakura, Y. Iwasawa, J. Catal. 127 (1991) 631.
[7] S. Naito, M. Tanimoto, J. Catal. 130 (1991) 106.
[8] A. Fusi, R. Psaro, C. Dossi, L. Garlaschelli, F. Cozzi, J. Mol. Catal. A 107 (1996) 255.
[9] T.A. Kainulainen, M.K. Niemelä, A.O.I. Krausc, J. Mol. Catal. A 140 (1999) 173.
[10] M. Ichikawa, A.J. Lang, D.F. Shriver, W.M.H. Sachtler, J. Am. Chem. Soc. 107 (1985) 7216.
[11] M. Lenarda, R. Ganzerla, L. Storaro, R. Zanoni, J. Mol. Catal. 78 (1993) 339.
[12] M. Lenarda, R. Ganzerla, L. Riatto, L. Storaro, J. Mol. Catal. A 187 (2002) 129.
[13] M. Ichikawa, J. Catal. 59 (1979) 67.
[14] L. Huang, Y. Xu, W. Guo, D. Li, X. Guo, Catal. Lett. 32 (1995) 61.
[15] A. Trunschke, H. Ewald, H. Miessner, A. Fukoka, M. Ichikawa, H.C. Böttcher, Mater. Chem. Phys. 29 (1991) 503.
[16] W.M.H. Sachtler, M. Ichikawa, J. Phys. Chem. 90 (1986) 4752.
[17] M. Ichikawa, L.F. Rao, T. Kimura, A. Fukoka, J. Mol. Catal. 62 (1990) 15.
[18] C. Dossi, S. Recchia, A. Fusi, Fresenius J. Anal. Chem. 367 (2000) 416.
[19] Report of the International Workshop on Standards and Criteria in XAFS, in: S.S. Hasnain (Eds.), X-Ray Absorption Fine Structure, Hellis Horwood, Chicester, 1991, p. 751.
[20] B. Lengeler, E.P. Eisenberger, Phys. Rev. B 21 (1980) 4507.
[21] A. Michalowicz (Ed.), Logiciel pour la Chemie, Soc. Francaise de Chemie, Paris, 1991, p. 102.
[22] F. James, M. Ross, MINUIT, CERN Computing Center, Program Library, CERN/DD Internal Report 75/20, 1976.
[23] R.W. Joyner, K.H. Martin, P. Meehan, J. Phys. C 20 (1987) 4005.
[24] R. Psaro, C. Dossi, A. Fusi, L. Sordelli, M. Graziani, CNR Rao (Eds.), Advances in Catalysis Design, vol. 2, World Science, Singapore, 1993, p. 303.
[25] K.J. Williams, M. Salmeron, A.T. Bell, G.A. Somorjiai, Catal. Lett. 1 (1983) 331.
[26] M.E. Levin, M. Salmeron, A.T. Bell, G.A. Somorjiai, J. Catal. 106 (1987) 401.
[27] A. Boffa, C. Lin, A.T. Bell, G.A. Somorjiai, J. Catal. 149 (1994) 149.
[28] T.G. Richmond, F. Basolo, D.F. Shriver, Inorg. Chem. 21 (1986) 1272.